ChemPubSoc Europe

DOI: 10.1002/chem.201400272

CHEMISTRY A European Journal Full Paper

Hybrid Materials

Nanostructured Graphene/TiO_2 Hybrids as High-Performance Anodes for Microbial Fuel Cells

Cui-e Zhao,[a] Wen-Jing Wang,[a] Dong Sun,[a] Xin Wang,[c] Jian-Rong Zhang,*[a, b] and Jun-Jie Zhu*[a]

Abstract: A new nanostructured graphene/TiO_2 (G/TiO_2) hybrid was synthesized by a facile microwave-assisted solvothermal process in which amorphous TiO_2 was assembled on graphene in situ. The resulting G/TiO_2 hybrids were characterized by XRD, SEM, TEM, Raman spectroscopy, and N_2 adsorption/desorption analysis. The electrochemical properties of the hybrids as anode materials for *Shewanella*-inoculated microbial fuel cells (MFCs) were studied for the first time, and they proved to be effective in improving MFC performance. The significantly improved bacterial attachment and extracellular electron-transfer efficiency could be attributed to the high specific surface area, active groups, large pore volume, and excellent conductivity of the nanostructured G/TiO_2 hybrid, and this suggests that it could be a promising candidate for high-performance MFCs.

Introduction

Microbial fuel cells (MFCs) are an emerging technology for electricity generation in which bacteria are used as catalysts to oxidize organic matter,[1] and have drawn extensive attention in fields such as wastewater treatment, bioremediation, and treatment of human excrement in space.[2] However, practical application of MFCs is still a challenge due to their low power output and low extracellular electron-transfer (EET) efficiency. Although a number of factors influence the performance of MFCs,[3] the anode material, which is associated with bacterial adhesion and electron transfer from microbes to the electrode by different mechanisms (cell surface proteins,[4] mediator compounds,[5] and conductive pili[6]), strongly influences the power density. Hence, numerous studies have been dedicated to improving anode materials for MFCs.

Commercially available carbon-based porous materials, such as carbon cloth, carbon paper, and carbon felt, have been widely used for MFCs because of their good chemical stability.[7] However, these materials usually exhibit poor bacterial adhesion and low EET efficiency. Moreover, the pores in these materials are easily clogged by rapid bacterial growth, which results in cell death and reduced surface area for electrochemical reaction. In general, there are two main ways to deal with these problems. One is to improve the electrode properties by surface treatment, for example, by means of ammonia treatment[8] or nanomaterial modification;[9] the other is to develop new anode materials with specific properties that improve the bacteria–electrode interactions at low cost to further improve the performance of MFCs.[10]

Titanium dioxide, as an important semiconductor material, has been extensively studied in many fields because of its advantages of rich abundance, low cost, nontoxicity, and chemical stability.[11] These properties make it particularly attractive for MFCs. However, the intrinsically low electrical conductivity of TiO_2 significantly restricts its application, because its low electron-transfer efficiency dramatically reduces the power output of MFCs. To overcome this drawback, the use of highly conductive additives to TiO_2, such as metals, metal oxides, and carbonaceous materials, has been proven to be an effective strategy to improve the electron-transfer efficiency of TiO_2.[12] Compared with other additives, graphene, a two-dimensional carbon material, seems particularly promising owing to its superior electrical conductivity, high specific surface area (theoretical value of 2600 $m^2 g^{-1}$), and excellent mechanical flexibility.[13] Importantly, the high surface area and functional groups of graphene sheets, especially when it is produced by chemical oxidation and thermal expansion of graphite, make it a competitive candidate. Consequently, the integration of TiO_2 with graphene is promising for MFC anode materials.

Herein, a new nanostructured G/TiO_2 hybrid was synthesized from graphene oxide (GO) and tetrabutyl titanate ($Ti(OBu)_4$) as starting materials in a one-step microwave-assisted solvother-

[a] C.-e. Zhao, W.-J. Wang, D. Sun, Prof. J.-R. Zhang, Prof. J.-J. Zhu
State Key Laboratory of Analytical Chemistry for Life Science
School of Chemistry and Chemical Engineering
Nanjing University, Nanjing 210093 (P.R. China)
E-mail: jrzhang@nju.edu.cn
jjzhu@nju.edu.cn

[b] Prof. J.-R. Zhang
School of Chemistry and Life Science, Nanjing University
Jinling College, Nanjing 210089 (P.R. China)

[c] Dr. X. Wang
MOE Key Laboratory of Pollution Processes and Environmental Criteria
Tianjin Key Laboratory of Environmental Remediation and Pollution Control
College of Environmental Science and Engineering
Nankai University, Tianjin 300071 (P.R. China)

Supporting information for this article is available on the WWW under http://dx.doi.org/10.1002/chem.201400272.

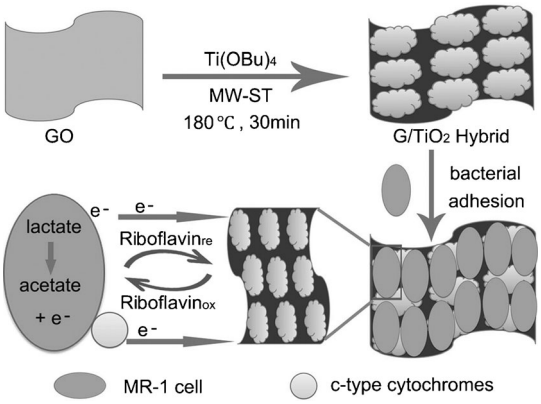

Scheme 1. Synthesis of nanostructured G/TiO_2 hybrids by a one-pot MWST process and their use as MFC anode materials.

mal (MWST) process (Scheme 1). GO could be easily reduced to graphene under the MWST conditions. Meanwhile, nanostructured TiO_2 was formed by hydrolysis of $Ti(OBu)_4$ and assembled in situ on the graphene sheets due to the large number of functional groups on graphene acting as active sites for its growth. By varying the weight ratio of GO and $Ti(OBu)_4$, several G/TiO_2 hybrids were obtained and explored as anode materials for MFCs. *Shewanella oneidensis* MR-1 (*S. oneidensis*), a dissimilatory metal-reducing bacterium that transfers electrons to an anode through c-type outer membrane cytochromes[14] and mediators (riboflavin molecules) excreted by itself,[15] was used as a model microbe in this study. The influence of different percentages of graphene in the G/TiO_2 hybrid anodes on the performance of MFCs was investigated. The G/TiO_2 hybrid with a graphene content of 20 wt% weight (denoted 20%G/TiO_2) proved effective in improving the MFC performance.

Results and Discussion

The crystal structure of the as-prepared samples was determined by XRD (Figure 1). The diffraction peak of GO around 9.5° (Figure 1a) was replaced by a broad peak at 23.5° after MWST treatment(Figure 1b), which is assigned to the (002) diffraction of graphene.[16] However, the absence of obvious XRD peaks for TiO_2 (Figure 1c) suggested that the sample was amorphous,[17] which may be ascribed to the rapid MWST process. The 20%G/TiO_2 hybrids (Figure 1d) showed an additional shoulder peak partially overlapping with the (101) peak of TiO_2, which is due to stacking of graphene in G/TiO_2. When the as-prepared 20%G/TiO_2 hybrid from the MWST process was subjected to further hydrothermal treatment at 200 °C for 20 h (Figure 1e and Figure S1 of the Supporting Information), the appearance of the diffraction peaks of anatase TiO_2 phase[18] indicated phase transition of amorphous TiO_2 to anatase TiO_2.

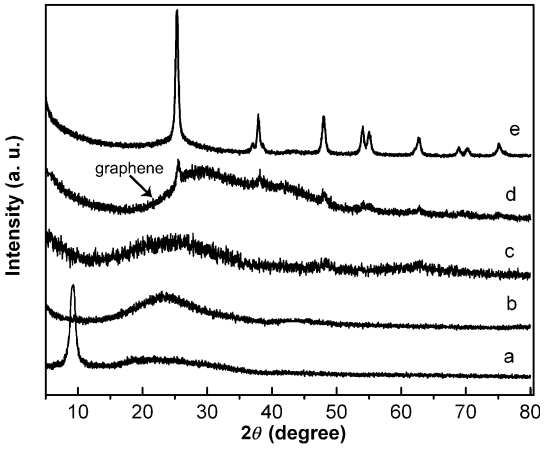

Figure 1. XRD patterns of a) GO, b) graphene, c) TiO_2, d) 20%G/TiO_2 hybrid, and e) 20%G/TiO_2 after hydrothermal treatment at 200 °C for 20 h.

Raman spectroscopy was performed to examine the G/TiO_2 hybrids. As shown in Figure 2, two broad peaks at about 1335 and 1596 cm^{-1} were observed for graphene (Figure 2a), which

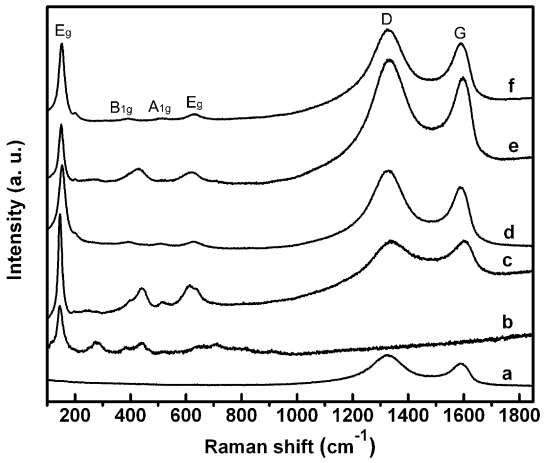

Figure 2. Raman spectra of a) graphene, b) TiO_2, c) 10%G/TiO_2, d) 20%G/TiO_2, e) 30%G/TiO_2, and f) 20%G/TiO_2 after hydrothermal treatment at 200 °C for 20 h.

can be assigned to the D and G bands of graphene, respectively. Moreover, the higher intensity of the D band compared to the G band indicates an increase in sp^2 domains and structural disorder of graphene sheets. The nanostructured TiO_2 exhibited characteristic Raman peaks (Figure 2b) around 143 (E_g), 276 (B_{1g}), 436 (A_{1g}), and 706 cm^{-1} (E_g), which are in good agreement with the Raman features of previously reported anatase TiO_2.[19] After incorporation of graphene, the E_g mode of TiO_2 shifted slightly from 143 to 148 cm^{-1} (Figure 2c–f), owing to the interaction of TiO_2 with graphene. Slight increases in the intensities of the D and G bands and variations in the measured peak frequencies among the samples with increasing amount of graphene in the hybrids revealed that the graphene is effectively integrated with TiO_2. Both as-synthesized and hydrothermally treated 20%G/TiO_2 exhibited similar Raman peaks, that is, 20%G/TiO_2 hybrids were successfully prepared by the MWST process.

The morphology of the G/TiO_2 hybrids was first investigated by field-emission SEM (FESEM). Figure 3A shows a typical SEM image of free-standing graphene nanosheets, which show wrinkled surfaces. In the SEM image of TiO_2 (Figure 3B), the

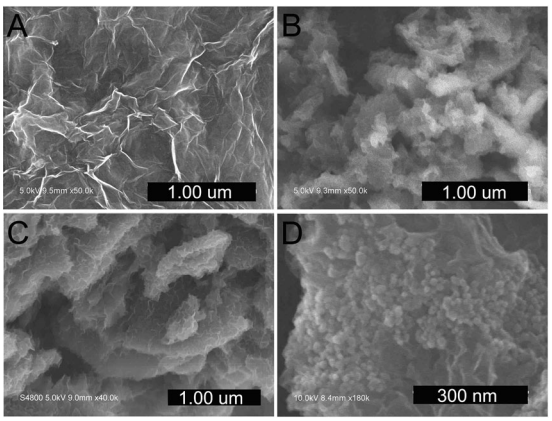

Figure 3. SEM images of A) graphene, B) TiO_2, C) 20%G/TiO_2 hybrid and D) 20%G/TiO_2 hybrid after hydrothermal treatment at 200 °C for 20 h.

nanostructure of amorphous TiO_2 can be observed. When graphene is introduced, the TiO_2 can uniformly grow on the surface of flexible graphene sheets to form G/TiO_2 hybrids (Figure 3C and Figure S2 of the Supporting Information), which suggests that the active groups on the graphene surface are favorable to the growth of TiO_2. Interestingly, after hydrothermal treatment, a large number of TiO_2 nanoparticles with an average diameter of about 30 nm were dispersed on the surface of graphene nanosheets (Figure 3D); this indicated that anatase TiO_2 had formed on the graphene. Elemental mapping of the as-synthesized 20%G/TiO_2 hybrid disclosed that C, O, and Ti were homogeneously distributed (Figure S3 in the Supporting Information). Energy-dispersive X-ray (EDX) analysis confirmed that the sample contained C, O, and Ti (Figure S4 in the Supporting Information).

The structure of the 20%G/TiO_2 hybrids was examined in further detail by high-resolution TEM (HRTEM). The HRTEM image in Figure 4A reveals that amorphous TiO_2 is loosely distributed on the graphene surface due to the large surface area of the graphene nanosheets.[20] Both the edge of a graphene sheet and the porous structure of TiO_2 are observable in the higher-magnification image (Figure 4B). After heat treatment, the graphene is well-decorated with spherical particles of anatase TiO_2 (Figure 4C). The selected-area electron diffraction (SAED) pattern of the hybrid is shown as an inset in Figure 4C, in which the well-defined diffraction lines can be indexed to the (101), (004), (200), and (211) planes of TiO_2,[19b] whereas the weak diffraction spots correspond to the (002) crystal plane of graphene. The higher-magnification TEM image (Figure 4D) clearly shows that the lattice fringes are separated by a spacing of about 0.35 nm, which is in accordance with the spacing of the (101) planes of anatase TiO_2.[21] In addition, the graphene sheets can be seen at the edge of the hybrid. Taken together, the results above demonstrate the successful integration of TiO_2 with graphene.

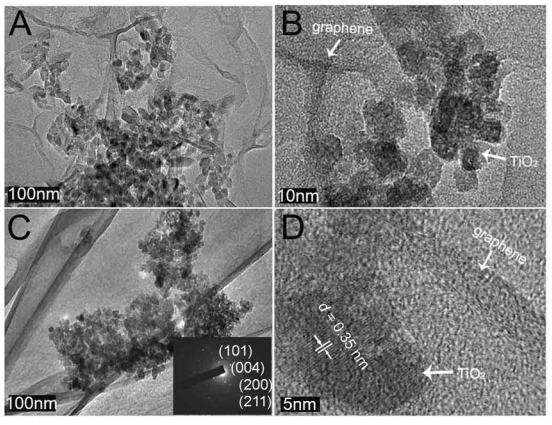

Figure 4. HRTEM images of the 20%G/TiO_2 hybrids before (A, B) and after (C, D) hydrothermal treatment at 200 °C for 20 h. Inset: SAED pattern.

The specific surface area and porous structure of the G/TiO_2 hybrids were investigated by measuring N_2 adsorption/desorption isotherms. The type IV isotherms and hysteresis loops of the samples (Figure 5) are characteristic of mesoporous materials.[22] The specific surface areas of the samples, calculated by the multipoint BET method, and the total pore volume, calculated by using the Barrett–Joyner–Halenda (BJH) equation, are listed in Table 1. The BET surface area of the graphene is only 2.39 $m^2 g^{-1}$, because pure graphene sheets are easily stacked. With increasing graphene content up to 20%, the BET surface area of the G/TiO_2 hybrids is enhanced from 205 to 319 $m^2 g^{-1}$. These values are significantly higher than those of reported

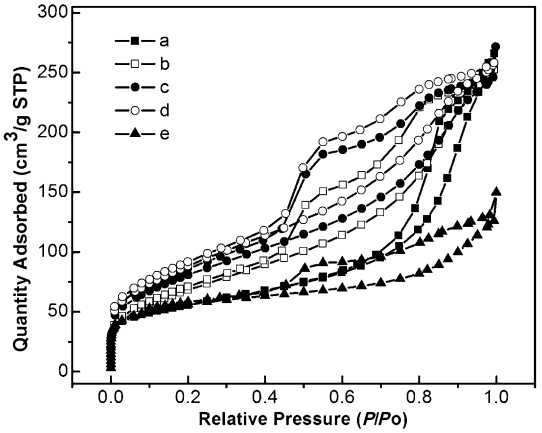

Figure 5. Nitrogen adsorption/desorption isotherms of a) TiO_2, b) 10%G/TiO_2, c) 20%G/TiO_2, d) 30%G/TiO_2, and e) 20%G/TiO_2 after hydrothermal treatment at 200 °C for 20 h.

Table 1. BET surface areas and BJH pore volumes of different samples.

Sample	S_{BET} [$m^2 g^{-1}$]	Total pore volume [$cm^{-3} g^{-1}$]
graphene	2.39	
TiO_2	205	0.775
10%G/TiO_2	279	0.549
20%G/TiO_2	319	0.587
30%G/TiO_2	332	0.545
20%G/TiO_2[a]	197	0.332

[a] Treated hydrothermally at 200 °C for 20 h.

TiO_2/graphene composites (100–200 $m^2 g^{-1}$)[11b, 13a, 23] and can be attributed to a synergistic effect between the amorphous TiO_2 and graphene. On one hand, the graphene sheets serve as a host substrate for in situ formation of amorphous TiO_2 and, on the other, the TiO_2 can effectively prevent the restacking of flexible graphene, which greatly increases the BET surface area. However, when the graphene content was increased to 30 wt%, no further increase in the BET surface area of G/TiO_2 hybrids was observed. The pore size distributions of the samples determined from the desorption branch of the isotherms are shown in Figure S5 (Supporting Information). The main pore size in the G/TiO_2 hybrids is around 2.5–5.0 nm, which is much smaller than the diameter of bacterial cells (ca. 0.5–2.0 μm). Thus, bacteria cannot enter the pores and clog them, which would cause their death from lack of nutrients. After hydrothermal treatment at 200 °C for 20 h, the BET surface area of the 20%G/TiO_2 hybrid decreased to 197 $m^2 g^{-1}$. The higher surface area provided by the as-synthesized 20%G/TiO_2 hybrid was expected to increase its ability to integrate with bacterial biofilms and to accept more electrons from mediators excreted by microbes. Moreover, such a highly porous structure is advantageous for electron collection from riboflavin molecules in solution and enhances electron transfer from bacteria to the electrode.

The electrochemical properties of the G/TiO_2 electrodes were evaluated by electrochemical impedance spectroscopy (EIS). All the electrodes showed similar Nyquist plots with a semicircle in the high-frequency region and a linear slope in the low-frequency region (Figure 6). The charge-transfer resistance R_{ct} at an electrode/electrolyte interface is usually indicated by the diameter of the semicircle in the Nyquist plot.[24] The R_{ct} value of graphene of only 3.5 Ω (Figure 6b) indicates high electrical conductivity. On incorporation of 10 wt% graphene, the R_{ct} of TiO_2 is remarkably reduced from about 900 to 35 Ω, so that the EET efficiency of the G/TiO_2 electrode is significantly enhanced after the introduction of graphene. A smaller R_{ct} value indicates a faster electron-transfer rate. However, when the graphene content in the G/TiO_2 hybrids increased from 20 to 30 wt%, the R_{ct} value only decreased from 14 to 12 Ω. As mentioned above, further increases in graphene content in the G/TiO_2 hybrids lower the pore volume of the nanostructured TiO_2 (Table 1), and this leads to decreased electron collection from mediators excreted by microbes.

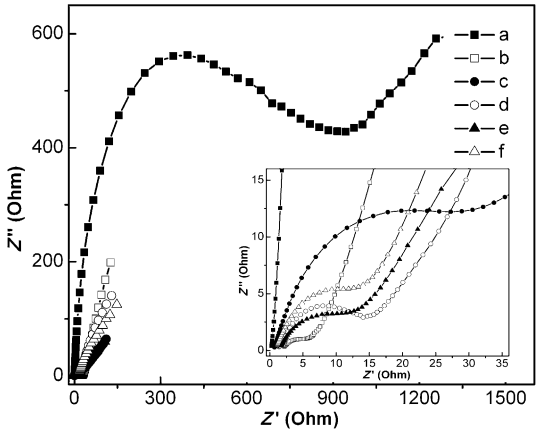

Figure 6. Nyquist plots from EIS studies on a) TiO_2, b) graphene, c) 10%G/TiO_2, d) 20%G/TiO_2, e) 30%G/TiO_2, and f) hydrothermally treated 20%G/TiO_2 for 20 h electrodes. Inset: higher-magnification view.

To investigate the influence of graphene content in the G/TiO_2 hybrids on the MFC performance, as-synthesized G/TiO_2 hybrid electrodes with different contents of graphene and the heat-treated 20%G/TiO_2 hybrid electrode were tested in a two-chamber MFC. The as-synthesized 20%G/TiO_2 anode has a higher output power density (ca. 268 $mW m^{-2}$) during discharge (Figure S6 in the Supporting Information), which indicates that it shows the best biocatalysis among the four anode materials. As discussed above, the as-synthesized 20%G/TiO_2 hybrid has a much higher active surface area than the hydrothermally treated 20%G/TiO_2 hybrid, which is beneficial to the attachment of bacterial cells and electron transfer between bacteria and the electrode. Moreover, it has a larger pore volume than the as-synthesized 30%G/TiO_2 hybrid, which will result in enhanced electron collection from mediators excreted by microbes. Thus, the as-synthesized 20%G/TiO_2 hybrid was selected as an anode material for MFCs.

To investigate the merits of the as-synthesized 20%G/TiO_2 hybrid as anode material in MFCs, the 20%G/TiO_2 hybrids before and after hydrothermal treatment, TiO_2-only, graphene-only, and a commonly used carbon-paper electrodes were incorporated in the anodic chamber of an MFC inoculated with *S. oneidensis* cells under the same conditions. After two weeks of operation, the morphology of the anodes was examined by SEM. The bacterial cells densely adhered to the surface of the as-synthesized 20%G/TiO_2 hybrid anode (Figure 7A), which in-

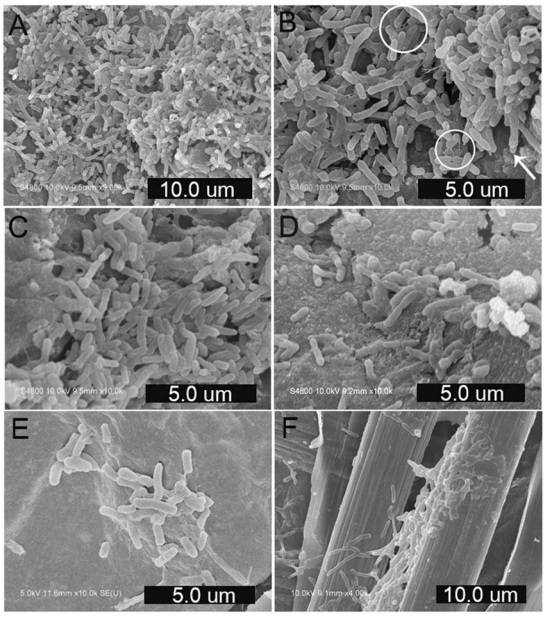

Figure 7. SEM images of bacterial cells adhering to as-synthesized 20%G/TiO_2 (A, B), TiO_2 (C), hydrothermally treated 20%G/TiO_2 (D), graphene (E), and carbon-paper (F) anodes.

dicates that it has good biocompatibility with bacteria. The high-magnification image (Figure 7B) reveals that bacterial cells are accumulated on the anode surface and cross-linked with each other to form a network by some pilus-like structures (circles), which are reported to play a key role in electron transfer and biofilm formation.[25] Moreover, compact attachment of cells to the 20%G/TiO_2 hybrid surface (arrow in Figure 7B) further improves the mechanical binding between cells and anode material. The as-synthesized TiO_2 anode also exhibited effective bacterial attachment (Figure 7C). In the case of the hydrothermally treated 20%G/TiO_2 hybrid anode, however, only a few bacterial cells were observed on the electrode surface (Figure 7D), owing to loss of active groups (hydroxyl or carboxyl) for bacterial attachment on heat treatment (Figure S7 of the Supporting Information). For the graphene anode, fewer bacterial cells were observed on the anode surface (Figure 7E). In the case of the carbon-paper anode, only a few bacterial cells were attached on the outer surface of the carbon fibers, and almost no cells were present on the interior fibers (Figure 7F). Both the as-synthesizedG/TiO_2 and TiO_2 anodes exhibit effective bacterial attachment, and thus abundant oxygen functional groups on the surface of the electrodes appear to play a significant role in bacterial-cell adhesion. To support this hypothesis, FTIR spectra of graphene, TiO_2, and 20%G/TiO_2 before and after hydrothermal treatment were compared (Figure S7 in the Supporting Information). Before heat treatment, the TiO_2 and 20%G/TiO_2 hybrid showed obvious peaks of oxygen functional groups, for example, O–H stretching around 3250 cm^{-1}, C–O stretching at 1060 cm^{-1}, and Ti-O-Ti stretching at low frequency ($<1000\ cm^{-1}$). However, after hydrothermal treatment, the absorption band around at 3250 cm^{-1} was no longer observed for the hydrothermally treated 20%G/TiO_2 hybrid, which indicates loss of active groups during hydrothermal treatment. Therefore, reduced bacterial attachment is observed on the hydrothermally treated 20%G/TiO_2 anode surface. These results suggest that the active groups and high surface area of the as-synthesized 20%G/TiO_2 hybrids are favorable to bacterial adhesion.

To further explore the utility of the as-synthesized 20%G/TiO_2 hybrids for MFCs, three biofilm-based bioanodes were analyzed by cyclic voltammetry (CV). As shown in Figure 8, no obvious redox peaks were observed in the CV plot of the carbon-paper anode, and this indicates that the carbon-paper electrode is not suitable for bacterial biofilm growth. In the case of the hydrothermally treated 20%G/TiO_2 anode, a weak but identifiable pair of redox peaks were observed at −0.482 and −0.436 V (vs. SCE), which are believed to originate from the c-type outer-membrane cytochromes of *Shewanella*, which are responsible for direct electron transfer between bacteria and the electrode.[26] The CV of the as-synthesized 20%G/TiO_2 hybrid anode exhibits one well-defined pair of redox peaks at potentials of −0.496 and −0.412 V, which are in accordance with the electrochemical response of the outer-membrane proteins of *Shewanella*. Furthermore, the peak current of the as-synthesized G/TiO_2 hybrid anode is higher than that of the hydrothermally treated G/TiO_2 anode or carbon-paper anode. The

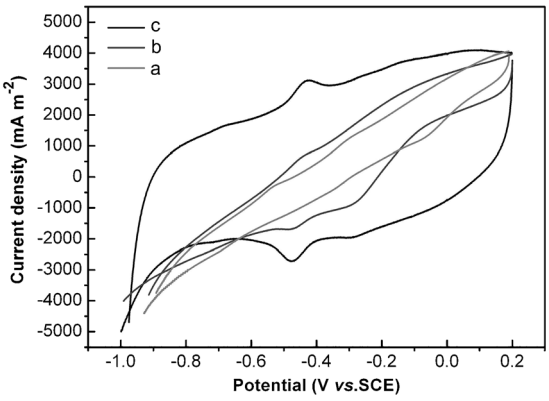

Figure 8. CV plots of biofilm-based carbon-paper (a), hydrothermally treated 20%G/TiO_2 (b), and as-synthesized 20%G/TiO_2 (c) bioanodes from MFCs in fresh mineral medium without substrate (potential range: −1.0 to 0.2 V, scan rate: 10 mV s^{-1}).

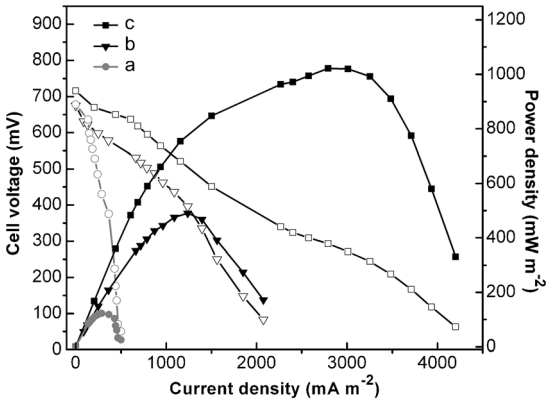

Figure 9. Polarization and power-density curves of the MFCs with a) carbon paper, b) hydrothermally treated 20%G/TiO_2, and c) as-synthesized 20%G/TiO_2 anodes.

results confirm that the as-synthesized 20%G/TiO_2 hybrid anode is promising for high-performance MFCs.

With high specific surface area, large pore volume, and high electron-transfer efficiency, the MFC equipped with the as-synthesized 20%G/TiO_2 hybrid anode was expected to provide a high power density output. The maximum power density of three different anodes were determined (Figure 9). The maximum power density of the as-synthesized 20%G/TiO_2 hybrid anode is 1060 mW m^{-2}, which is 1.6 and 7.8 times higher than those of the hydrothermally treated 20%G/TiO_2 anode (409 mW m^{-2}) and the carbon-paper anode (120 mW m^{-2}), respectively. The power density of the as-synthesized 20%G/TiO_2 hybrid anode is higher than those of previously reported *Shewanella*-catalyzed MFC anodes under similar conditions,[27] which further demonstrates that the as-synthesized 20%G/TiO_2 hybrid could be a superior anode material for MFCs.

Conclusion

A nanostructured G/TiO_2 hybrid was synthesized by a one-step MWST process, and for the first time used as anode material

for MFCs. In the G/TiO_2 hybrids, the amorphous TiO_2 could effectively prevent restacking of flexible graphene sheets, while the graphene served as a host substrate for the formation of nanostructured TiO_2 with greatly increased BET surface area and electrical conductivity. The as-synthesized20%G/TiO_2 hybrid anode exhibited effective bacterial adhesion and high power density in MFCs due to synergistic integration of TiO_2 and graphene, and thus it has potential applications as a high-performance anode material for MFCs.

Experimental Section

Materials and chemicals

Graphite powder (KS-10) was obtained from Sigma-Aldrich. GO was prepared from natural graphite powder according to the modified Hummers method and purified as described previously,[28] and then dispersed in water by ultrasonication (100 W, 40 kHz). $Ti(OBu)_4$ was obtained from Nanjing Chemical Co. (China). All reagents were of analytical reagent grade and used as received. Ultrapure water (18.2 MΩ cm at 25 °C) prepared with a Milli-Q system was used throughout all experiments.

Apparatus

An MWST synthesis system (CEM Discover, USA), equipped with controllable temperature and pressure units, was used for the preparation of G/TiO_2 hybrids. The morphology of the samples was examined by FESEM (Hitachi S4800) and HRTEM (JEM-2010F). EDX and elemental mapping were conducted by SEM. XRD measurements were performed on a Japan Shimadzu XRD-6000 powder X-ray diffractometer with $Cu_{K\alpha}$ radiation ($\lambda = 1.5405$ Å). Raman spectra were obtained with a confocal Raman Spectrometer (Renishaw invia Raman microscope) with an excitation wavelength of 633 nm. Nitrogen adsorption/desorption isotherms were measured at 77 K (ASAP 2010). EIS was carried out with an Autolab PGSTAT12 (Metrohm/Eco Chemie, BV, The Netherlands) in suspensions of bacterial cells at open-circuit potential. The frequency range was between 10^{-2} and 10^5 Hz. CV analysis was performed on a CHI660D electrochemical workstation (Chenhua, China) with an SCE reference electrode and a platinum counter electrode.

Synthesis of G/TiO_2 hybrids

In a typical preparation process, nanostructured G/TiO_2 hybrids were synthesized by a facile one-pot MWST method with an aqueous suspension of GO and tetrabutyl titanate as starting materials in ethanol/water. Briefly, 20 mg of GO was first dispersed in 20 mL of water by ultrasonic treatment to create a 1.0 mg mL^{-1} dispersion (component A). Component B was prepared by adding first 80 mg of tetrabutyl titanate and then 5 mL of $NH_3 \cdot H_2O$ to 5 mL of ethanol. Subsequently, component B was gradually dropped into component A and the mixture was sonicated for 30 min. The mixture was then heated by the MWST method at 180 °C/160 psi for 30 min, and the as-synthesized products were collected by centrifugation and washed with water several times. Finally, the samples were dried at 60 °C for 12 h for further characterization. For comparison, pure graphene and pure TiO_2 were prepared under the same conditions in the absence of tetrabutyl titanate and GO, respectively. To obtain the hydrothermally treated 20%G/TiO_2, the as-prepared 20%G/TiO_2 hybrid was subjected to hydrothermal conditions at 200 °C for 20 h.

Preparation of electrodes

The working electrodes were prepared by mixing the TiO_2 or G/TiO_2 hybrid powders with a PTFE solution and pasting them onto the surface of nickel foams (1×1 cm (two sides) = 2 cm^2) with a loading of about 5.0 mg cm^{-2} to produce uniform films, and pressed and dried at 120 °C for 12 h. Then, the electrodes were used as anodes for MFCs.

MFC construction and operation

H-shaped dual-chamber MFCs were constructed by connecting two glass bottles with a 30 mm diameter tube. The *S. oneidensis* cells harvested at late stationary phase were inoculated into the MFC anode chamber containing 100 mL of M9 buffer solution with 5% Luria–Bertani (LB) broth and 18 mM lactate as the electron donor. The anode chambers were maintained under anaerobic conditions. The catholyte was 50 mM $K_3Fe(CN)_6$ in 100 mM phosphate buffer (PBS, pH 7.4) solution, and carbon paper (2×2 cm (two sides) = 8 cm^2) was used as the cathode. The anode and the cathode chambers were separated by a proton-exchange membrane (Nafion 211, DuPont), and connected to an external resistance of 1000 Ω with titanium wire. The voltage was recorded with a multimeter. The polarization and power-density curves were obtained by varying the external resistance (50–9000 Ω) applied to the circuit and using a multimeter to measure the cell voltage. Current I was calculated as $I = E/R$, and power P was calculated as $P = IE$, where E is the cell voltage. The current and power densities were then normalized to the surface area of the anode. *S. oneidensis* cells were cultivated aerobically at 37 °C in 5 mL of LB broth for 12 h, and then the strain was subcultured at 30 °C and agitated at a rate of 150 rpm for 24 h. The cells were harvested at late stationary phase by centrifugation (6000 rpm, 5 min), washed three times with PBS, and then suspended in the MFC anode chamber. M9 buffer solution was composed of 22 mM KH_2PO_4, 42 mM Na_2HPO_4, 85.5 mM NaCl, and 1.0 mM $MgSO_4$. All media were sterilized before use.

SEM characterization of bioanodes

The bioanodes were removed from anode chamber of the MFC and immediately fixed in 2.5% glutaraldehyde solution for 2 h, washed three times with PBS, and dehydrated in a graded series of aqueous ethanol solutions (25, 50, 75, 95, and 100%) for 10 min each. The samples were then dried to remove residual moisture and coated with Au prior to SEM observation.

Acknowledgements

We gratefully appreciate the National Natural Science Foundation (21175065, 21121091, and 31272081), the National Basic Research Program (2011CB933502), and the Scientific Research Foundation of Graduate School of Nanjing University (2011 CL05).

Keywords: fuel cells · graphene · microwave chemistry · solvothermal synthesis · titania

[1] B. E. Logan, B. Hamelers, R. Rozendal, U. Schröder, J. Keller, S. Freguia, P. Aelterman, W. Verstraete, K. Rabaey, *Environ. Sci. Technol.* **2006**, *40*, 5181–5192.
[2] D. R. Lovley, *Nat. Rev. Microbiol.* **2006**, *4*, 497–508.
[3] a) I. S. Chang, H. Moon, O. Bretschger, J. K. Jang, H. I. Park, K. H. Nealson, B. H. Kim, *J. Microbiol. Biotechnol.* **2006**, *16*, 163–177; b) Y. Qiao, S. J.

Bao, C. M. Li, *Energy Environ. Sci.* **2010**, *3*, 544 – 553; c) W.-W. Li, G.-P. Sheng, X.-W. Liu, P.-J. Cai, M. Sun, X. Xiao, Y.-K. Wang, Z.-H. Tong, F. Dong, H.-Q. Yu, *Biosens. Bioelectron.* **2011**, *26*, 3987 – 3992; d) H. Liu, S. Cheng, B. E. Logan, *Environ. Sci. Technol.* **2005**, *39*, 5488 – 5493.

[4] L. Shi, D. J. Richardson, Z. Wang, S. N. Kerisit, K. M. Rosso, J. M. Zachara, J. K. Fredrickson, *Environ. Microbiol. Rep.* **2009**, *1*, 220 – 227.

[5] M. Adachi, T. Shimomura, M. Komatsu, H. Yakuwa, A. Miya, *Chem. Commun.* **2008**, *0*, 2055 – 2057.

[6] G. Reguera, K. D. McCarthy, T. Mehta, J. S. Nicoll, M. T. Tuominen, D. R. Lovley, *Nature* **2005**, *435*, 1098 – 1101.

[7] J. Liu, Y. Qiao, C. X. Guo, S. Lim, H. Song, C. M. Li, *Bioresour. Technol.* **2012**, *114*, 275 – 280.

[8] S. Cheng, B. E. Logan, *Electrochem. Commun.* **2007**, *9*, 492 – 496.

[9] a) Y. Zhao, K. Watanabe, R. Nakamura, S. Mori, H. Liu, K. Ishii, K. Hashimoto, *Chem. Eur. J.* **2010**, *16*, 4982 – 4985; b) J. Hou, Z. Liu, P. Zhang, *J. Power Sources* **2013**, *224*, 139 – 144; c) L. Peng, S.-J. You, J.-Y. Wang, *Biosens. Bioelectron.* **2010**, *25*, 1248 – 1251.

[10] a) Z. He, J. Liu, Y. Qiao, C. M. Li, T. T. Y. Tan, *Nano lett.* **2012**, *12*, 4738 – 4741; b) X. Xie, G. Yu, N. Liu, Z. Bao, C. S. Criddle, Y. Cui, *Energy Environ. Sci.* **2012**, *5*, 6862 – 6866; c) Y. Qiao, S.-J. Bao, C. M. Li, X.-Q. Cui, Z.-S. Lu, J. Guo, *ACS Nano* **2008**, *2*, 113 – 119; d) S. Chen, H. Hou, F. Harnisch, S. A. Patil, A. A. Carmona-Martinez, S. Agarwal, Y. Zhang, S. Sinha-Ray, A. L. Yarin, A. Greiner, U. Schroder, *Energy Environ. Sci.* **2011**, *4*, 1417 – 1421; e) S. Chen, G. He, X. Hu, M. Xie, S. Wang, D. Zeng, H. Hou, U. Schröder, *ChemSusChem* **2012**, *5*, 1059 – 1063.

[11] a) D. Wang, D. Choi, J. Li, Z. Yang, Z. Nie, R. Kou, D. Hu, C. Wang, L. V. Saraf, J. Zhang, I. A. Aksay, J. Liu, *ACS Nano* **2009**, *3*, 907 – 914; b) X. Xin, X. Zhou, J. Wu, X. Yao, Z. Liu, *ACS Nano* **2012**, *6*, 11035 – 11043.

[12] a) J. Liu, J. Xu, R. Che, H. Chen, M. Liu, Z. Liu, *Chem. Eur. J.* **2013**, *19*, 6746 – 6752; b) N. Yang, Y. Liu, H. Wen, Z. Tang, H. Zhao, Y. Li, D. Wang, *ACS Nano* **2013**, *7*, 1504 – 1512; c) L. Gu, J. Wang, H. Cheng, Y. Zhao, L. Liu, X. Han, *ACS Appl. Mater. Interfaces* **2013**, *5*, 3085 – 3093.

[13] a) N. Li, G. Liu, C. Zhen, F. Li, L. Zhang, H.-M. Cheng, *Adv. Funct. Mater.* **2011**, *21*, 1717 – 1722; b) J. Shen, B. Yan, M. Shi, H. Ma, N. Li, M. Ye, *J. Mater. Chem.* **2011**, *21*, 3415 – 3421; c) Y. Wu, Z. Wen, H. Feng, J. Li, *Chem. Eur. J.* **2013**, *19*, 5631 – 5636; d) H. Zhang, X. Lv, Y. Li, Y. Wang, J. Li, *ACS Nano* **2010**, *4*, 380 – 386.

[14] J. K. Fredrickson, M. F. Romine, A. S. Beliaev, J. M. Auchtung, M. E. Driscoll, T. S. Gardner, K. H. Nealson, A. L. Osterman, G. Pinchuk, J. L. Reed, D. A. Rodionov, J. L. M. Rodrigues, D. A. Saffarini, M. H. Serres, A. M. Spormann, I. B. Zhulin, J. M. Tiedje, *Nat. Rev. Microbiol.* **2008**, *6*, 592 – 603.

[15] E. Marsili, D. B. Baron, I. D. Shikhare, D. Coursolle, J. A. Gralnick, D. R. Bond, *Proc. Natl. Acad. Sci. USA* **2008**, *105*, 3968 – 3973.

[16] K. Liu, J.-J. Zhang, F.-F. Cheng, T.-T. Zheng, C. Wang, J.-J. Zhu, *J. Mater. Chem.* **2011**, *21*, 12034 – 12040.

[17] P. Si, S. Ding, J. Yuan, X. W. Lou, D.-H. Kim, *ACS Nano* **2011**, *5*, 7617 – 7626.

[18] a) J. S. Chen, Y. L. Tan, C. M. Li, Y. L. Cheah, D. Luan, S. Madhavi, F. Y. C. Boey, L. A. Archer, X. W. Lou, *J. Am. Chem. Soc.* **2010**, *132*, 6124 – 6130; b) J. M. Lee, I. Y. Kim, S. Y. Han, T. W. Kim, S.-J. Hwang, *Chem. Eur. J.* **2012**, *18*, 13800 – 13809.

[19] a) V. Štengl, D. Popelková, P. Vláčil, *J. Phys. Chem. A J. Phys. Chem. B J. Phy. Chem. C.* **2011**, *115*, 25209 – 25218; b) B. Jiang, C. Tian, W. Zhou, J. Wang, Y. Xie, Q. Pan, Z. Ren, Y. Dong, D. Fu, J. Han, H. Fu, *Chem. Eur. J.* **2011**, *17*, 8379 – 8387.

[20] S. Ding, J. S. Chen, D. Luan, F. Y. C. Boey, S. Madhavi, X. W. Lou, *Chem. Commun.* **2011**, *47*, 5780 – 5782.

[21] Q. Min, X. Zhang, H. Zhang, F. Zhou, J.-J. Zhu, *Chem. Commun.* **2011**, *47*, 11709 – 11711.

[22] L. Shen, X. Zhang, H. Li, C. Yuan, G. Cao, *J. Phy. Chem. Lett.* **2011**, *2*, 3096 – 3101.

[23] S. Yang, X. Feng, K. Müllen, *Adv. Mater.* **2011**, *23*, 3575 – 3579.

[24] Z. He, F. Mansfeld, *Energy Environ. Sci.* **2009**, *2*, 215 – 219.

[25] J. L. Telford, M. A. Barocchi, I. Margarit, R. Rappuoli, G. Grandi, *Nat. Rev. Microbiol.* **2006**, *4*, 509 – 519.

[26] a) K. Fricke, F. Harnisch, U. Schroder, *Energy Environ. Sci.* **2008**, *1*, 144 – 147; b) L. Deng, S. Guo, Z. Liu, M. Zhou, D. Li, L. Liu, G. Li, E. Wang, S. Dong, *Chem. Commun.* **2010**, *46*, 7172 – 7174; c) A. A. Carmona-Martinez, F. Harnisch, L. A. Fitzgerald, J. C. Biffinger, B. R. Ringeisen, U. Schröder, *Bioelectrochemistry* **2011**, *81*, 74 – 80; d) C. Zhao, Y. Wang, F. Shi, J. Zhang, J.-J. Zhu, *Chem. Commun.* **2013**, *49*, 6668 – 6670.

[27] a) Y.-C. Yong, X.-C. Dong, M. B. Chan-Park, H. Song, P. Chen, *ACS Nano* **2012**, *6*, 2394 – 2400; b) Y.-Y. Yu, H.-I. Chen, Y.-C. Yong, D.-H. Kim, H. Song, *Chem. Commun.* **2011**, *47*, 12825 – 12827.

[28] Y. Xu, H. Bai, G. Lu, C. Li, G. Shi, *J. Am. Chem. Soc.* **2008**, *130*, 5856 – 5857.

Received: January 23, 2014
Published online on April 17, 2014

